Controls on Sea-Air CO_2 Flux in EBUS

Riley X. Brady

June 12, 2017

Abstract

Working to understand what controls historical variability in Sea-Air CO_2 Flux in Eastern Boundary Upwelling Systems. I use FG_CO2 output from the CESM Large Ensemble and correlate it to various climate indices derived from model output.

1 California Current

1.1 Study Site

For simplicity, I am using the latitudinal bounds set up by Chavez and Messié [2009]. This equates to 34N - 44N for the CCS. In terms of longitude, I want to approach it similarly to Turi et al. [2014]. In the future, I can make this banded if needed (0-100km, 100-400km, etc.), but for now, 4 regions by 3 bands per region is a lot to work with. Instead, I am just restricting it to 800km offshore and bounded by 10 degrees of latitude for standardization.

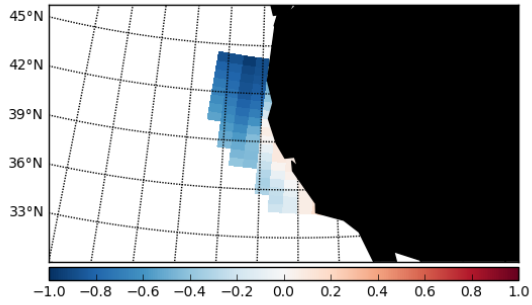

Figure 1: Time-averaged (1920-2015) and ensemble-averaged sea-air CO_2 flux (FGCO2). Simply depicting the region over which time series are analyzed/correlated with respect to climate indices.

1.2 Time Series Filtering

Here, the intent is to correlate a monthly time series of FGCO2 with monthly climate indices from the CVDP output (spanning 1920-2015). At first glance, the FGCO2 output is much too noisy.

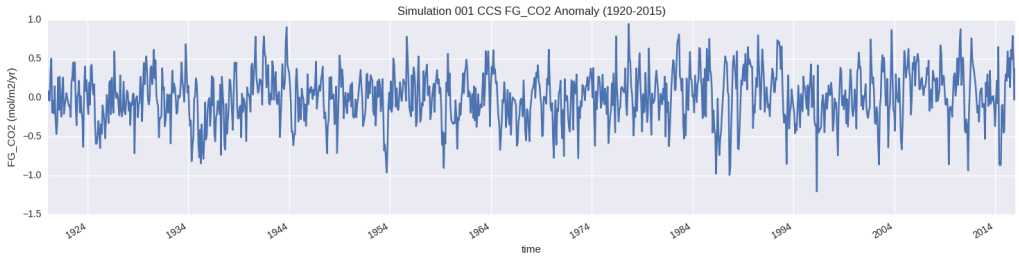

Figure 2: Area-weighted average FGCO2 anomalies (ensemble mean removed) for simulation 001 over the domain in Figure 1.

We can apply a quick 12-month (annual) rolling mean to smooth out some of the noisiness. Figure 3 shows the smoothed time series in black for simulation 001 (with the original unfiltered time series from Figure 2 in blue). We only lose 11 data points on a 1140 length array by smoothing.

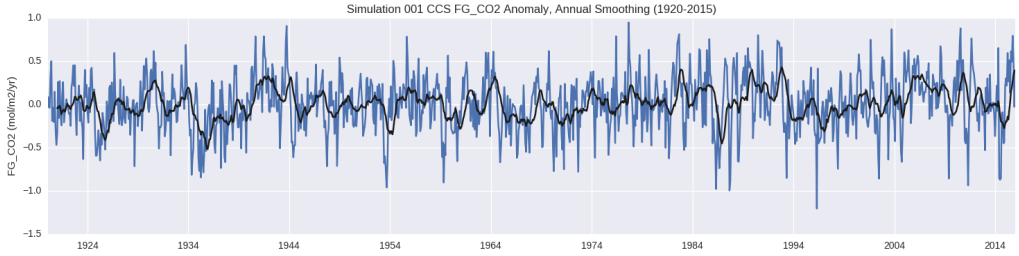

Figure 3: Area-weighted average FGCO2 anomalies (ensemble mean removed) for simulation 001 over the domain in Figure 1.

An FFT of Figure 2 is fairly inconclusive. At the very least, there is power at lower frequencies that diminishes at higher frequencies. It looks more red than white.

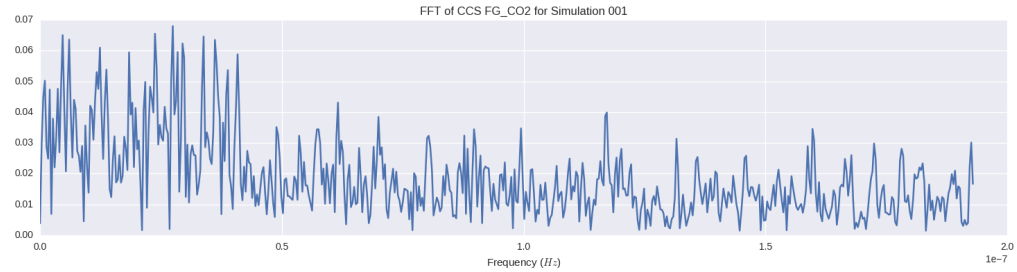

Figure 4: Area-weighted average FGCO2 anomalies (ensemble mean removed) for simulation 001 over the domain in Figure 1.

Now smoothed, the FGCO2 anomalies vary more closely with the Nino3.4 index, and even moreso with the PDO index.

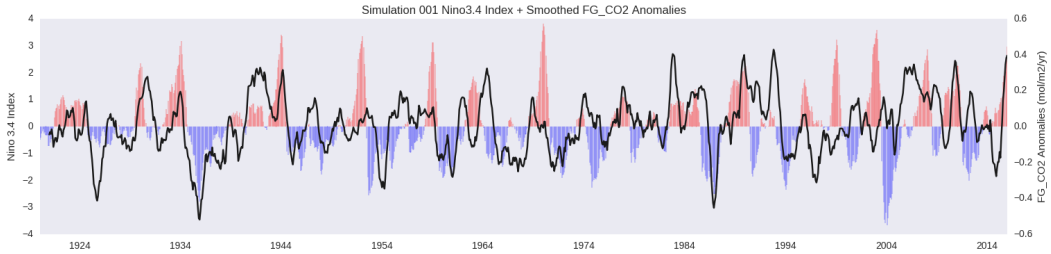

Figure 5: Area-weighted average FGCO2 anomalies for simulation 001 with a one-year moving average applied (black line). The bar plot reflects the detrended Nino3.4 index from the same simulation.

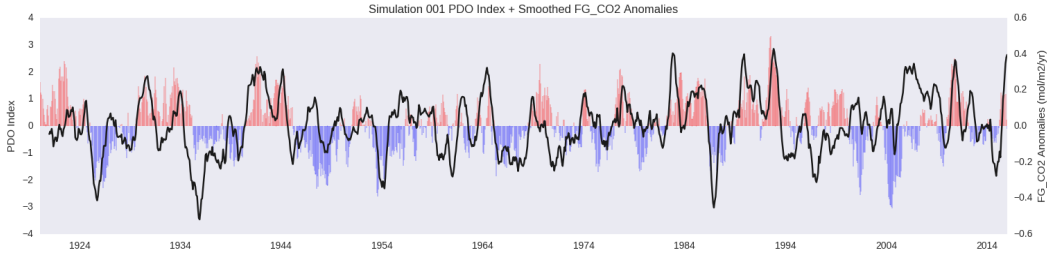

Figure 6: Same as Figure 5, but with the PDO index.

1.3 Regressing onto Climate Indices

I can now regress these smoothed FGCO2 anomalies onto three main predictors: Nino3.4, PDO, and NPO (the last of which isn't covered here due to low correlation values). Figure 7 displays a scatter plot for all 34 ensemble members comparing their r-value for ENSO to their r-value for PDO. Save for one outlier in the bottom left, simulations cluster generally toward strong correlations for both metrics, favoring the PDO index. Table 1 and Table 2 display raw results (R value, R^2, and regression coefficient) for every simulation.

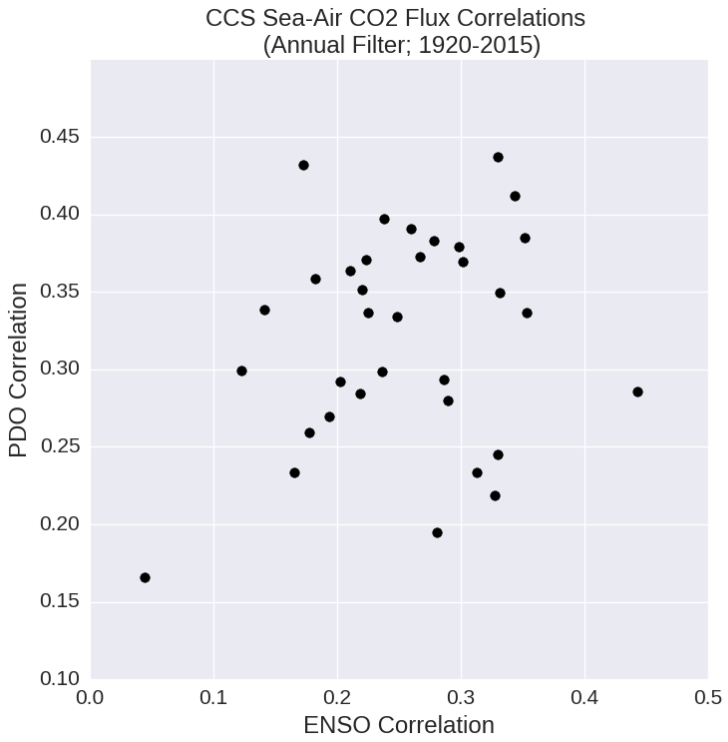

Figure 7: R values for annually smoothed FGCO2 anomalies in the CCS compared to Nino3.4 and PDO indices for all 34 ensemble members.

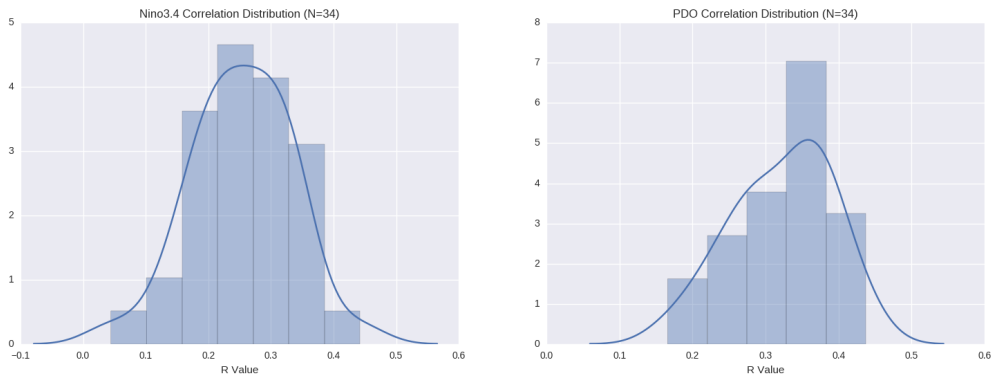

Figure 8: Distribution of correlations between smoothed FGCO2 anomalies and Nino3.4/PDO indices.

Table 1: Regression Results by simulation, with Nino3.4 index as the predictor and FGCO2 anomalies as the criterion. All results have a p-value << 0.05.

Simulation	**Slope** [mol/m^2/yr/degC]	**R**	**R^2**
001	0.04	0.30	0.09
002	0.06	0.33	0.11
009	0.03	0.18	0.03
010	0.04	0.22	0.05
011	0.01	0.04	0.00
012	0.05	0.28	0.08
013	0.06	0.33	0.11
014	0.05	0.35	0.12
015	0.05	0.29	0.08
016	0.04	0.22	0.05
017	0.04	0.27	0.07
018	0.05	0.29	0.08
019	0.04	0.21	0.04
020	0.05	0.30	0.09
021	0.03	0.18	0.03
022	0.04	0.24	0.06
023	0.03	0.22	0.05
024	0.06	0.33	0.11
025	0.05	0.34	0.12
026	0.04	0.25	0.06
027	0.04	0.28	0.08
028	0.03	0.17	0.03
029	0.05	0.33	0.11
030	0.03	0.19	0.04
031	0.04	0.24	0.06
032	0.04	0.20	0.04
033	0.02	0.14	0.02
034	0.06	0.31	0.10
035	0.03	0.17	0.03
101	0.07	0.44	0.20
102	0.04	0.26	0.07
103	0.04	0.22	0.05
104	0.05	0.35	0.12
105	0.02	0.12	0.01
Mean	0.04	0.25	0.07
Std. Dev	0.01	0.08	0.04

Table 2: Same as Table 1, but as compared to the PDO index

Simulation	**Slope** [mol/m^2/yr/degC]	**R**	**R^2**
001	0.06	0.38	0.14
002	0.06	0.35	0.12
009	0.06	0.36	0.13
010	0.06	0.35	0.12
011	0.03	0.17	0.03
012	0.07	0.38	0.15
013	0.04	0.25	0.06
014	0.06	0.34	0.11
015	0.05	0.29	0.09
016	0.05	0.28	0.08
017	0.06	0.37	0.14
018	0.05	0.28	0.08
019	0.07	0.36	0.13
020	0.06	0.37	0.14
021	0.04	0.26	0.07
022	0.07	0.40	0.16
023	0.05	0.37	0.14
024	0.08	0.44	0.19
025	0.07	0.41	0.17
026	0.05	0.33	0.11
027	0.03	0.19	0.04
028	0.07	0.43	0.19
029	0.03	0.22	0.05
030	0.05	0.27	0.07
031	0.05	0.30	0.09
032	0.05	0.29	0.09
033	0.05	0.34	0.11
034	0.04	0.23	0.05
035	0.04	0.23	0.05
101	0.05	0.29	0.08
102	0.07	0.39	0.15
103	0.06	0.34	0.11
104	0.06	0.39	0.15
105	0.05	0.30	0.09
Mean	0.05	0.32	0.11
Std. Dev	0.01	0.07	0.04

References

Francisco P Chavez and Monique Messié. A comparison of eastern boundary upwelling ecosystems. *Progress in Oceanography*, 83(1):80–96, 2009.

G. Turi, Z. Lachkar, and N. Gruber. Spatiotemporal variability and drivers of pco_2 and air–sea co_2 fluxes in the california current system: an eddy-resolving modeling study. *Biogeosciences*, 11(3):671–690, 2014. doi: 10.5194/bg-11-671-2014. URL `http://www.biogeosciences.net/11/671/2014/`.